University of Groningen

Faculty of Mathematics
and Natural Sciences
Applied Physics

Physics of Nanodevices

Hot electron attenuation length of $NiSi_2$ on n-Si(111)

Bachelor Thesis by: Pieter Klandermans

Supervisors: Subir Parui, dr. Tamalika Banerjee

Group leader: prof. dr. ir. Bart J. van Wees

university of groningen

faculty of mathematics and natural sciences

April - July 2011

Abstract

In this Bachelor thesis the hot electron attenuation length of $NiSi_2$ on n-Si(111) is presented. For the preparation of $NiSi_2$/Si epitaxial interfaces, a flat and passivated Si(111) substrate is needed. Preparing this substrate is done by wet chemical etching in BHF, 1%HF and 40%NH_4F. An optimization in the time to remove the dissolved oxygen and the etching time is investigated. The starting point for our device fabrication was a passivated surface with an overall RMS roughness 5 Å and around 2 Åin smaller locations. This substrate was used to grow epitaxially type-A $NiSi_2$ using molecular beam epitaxy (MBE). The hot electron attenuation length could be derived from samples with varying thickness of $NiSi_2$ and measuring the transmission with ballistic electron emission microscopy (BEEM). The samples were in the range of 3.25 to 22.5 nm $NiSi_2$. It was shown that the attenuation length is energy dependent.

Contents

Chapter 1

Introduction

The preparation of atomically flat, well ordered, clean and passivated silicon surface is of great interest to the semiconductor industry. Understanding and optimizing the protocol to fabricate a flat and clean Si surface, in this case n-Si(111), is essential to realize better device performance. In this report, the surface preparation of n-Si(111) by wet chemical etching is studied to search for the optimized recipe to create Si surfaces. Preparation of Si(111) surface resulting in the presence of only Si(111) planes on the top surface is more involved than the preparation of a Si(100) surface. It involves the use of 40%NH_4F for etching, accompanied by bubbling with Nitrogen gas to remove dissolved oxyygen. In this work optimization of the etching time by 40%NH_4F and the gas bubbling time were extensively investigated in different Si substrates. The surface morphology was investigated during the optimization process with the atomic force microscope (AFM).

The optimized Si surface was then used to fabricate Metal-Semiconductor devices (M-S) with $NiSi_2$. This $NiSi_2$ can grow epitaxially on Si making use of molecular beam epitaxy (MBE) with a low lattice mismatch and good electrical properties. Because $NiSi_2$ is thermally stable it can be integrated into Si processing which requires high temperatures. Using $NiSi_2$/Si interfaces as building blocks to study spin transport in metallic systems is a current research topic in the group [1]. Using ballistic-electron-emission-microscopy (BEEM), the electron transmission through the thin film and across such interfaces can be studied. The hot electron attenuation length in epitaxial $NiSi_2$ has also been studied using such optimized interfaces. This is done by varying the thickness of $NiSi_2$ and measuring the transmission at different energies using BEEM.This is done by varying the thickness of $NiSi_2$ and measuring the transmission at different energies using BEEM. The understanding of this electronic transport property is essential to understand the spin transport in spin valves using such $NiSi_2$/n-Si Schottky diodes.

Outline

In chapter 2 the theory of BEEM, Schottky Barriers and the properties of Si(111) and $NiSi_2$ will be discussed. Chapter 3 contains the preparation and measurement of n-Si(111) and $NiSi_2$ samples. The results, mostly AFM images for the Si(111) and BEEM transmission spectra for $NiSi_2$, are discussed in chapter 4. The conclusions and recommendations are presented in chapter 5.

Chapter 2

Theory

2.1 BEEM

Since Kaiser and Bell demonstrated in 1988 [2] the technique of ballistic-electron-emission microscopy (BEEM), this technique is widely used in studying electronic transport across M-S interfaces as well as for imaging subsurface interface properties across such interfaces, non destructively [3]. BEEM is based on the technique of the Scanning Tunneling Microscope (STM) and uses the STM tip to inject hot electrons into the a metallic overlayer when a tunnel voltage V_T is applied between the tip and the overlayer. The electrons travel through the metal-base layer and reach the semiconductor which is used as a collector. If the applied tunnel voltage is greater than the barrier height at the M-S interface, the electrons cross the interface into the semiconductor and results in a collector current I_B. A voltage lower than the threshold voltage will result in no ballistic-electron current into the collector and will result in the electrons scattering back into the metal base (Figures 2.1a and 2.1b). The collector current as a function of the tip voltage can be used to study interface properties such as Schottky Barrier Height (SBH) and details of transport mechanisms at higher energies and on the nanoscale. An image of the local variation in the collector current can be obtained by scanning the tip over a certain area [2–5]. Other restriction for the electrons to cross the barrier are the availability of final states available in the substrate and the constraints whether the kinematics (i.e. both energy and momentum conservation) governing the particular MS-interface are satisfied [6].

2.1.1 Attenuation length

The BEEM current is strongly dependent on scattering events in the metal overlayer,at the M-S interface and within the semiconductor. So to understand the BEEM data, a fundamental understanding of the different kind of scattering processes is essential. Electrons can scatter elastically off defect sites or inelastic electron-electron scattering near the Fermi level. In general, inelastic scattering by electron-hole pair creation (electron-electron interaction) involves large energy loss [6]. Elastic scattering will only change the momentum (k-vector), but no energy will be lost or gained (for example, by impurity and defect scattering). Also semielastic scattering from phonons is possible. Phonon scattering in a metal appears to be insignificant in comparison to e^--e^- scattering for hot carriers. e^--e^- scattering will cause energy loss in a hot elec-

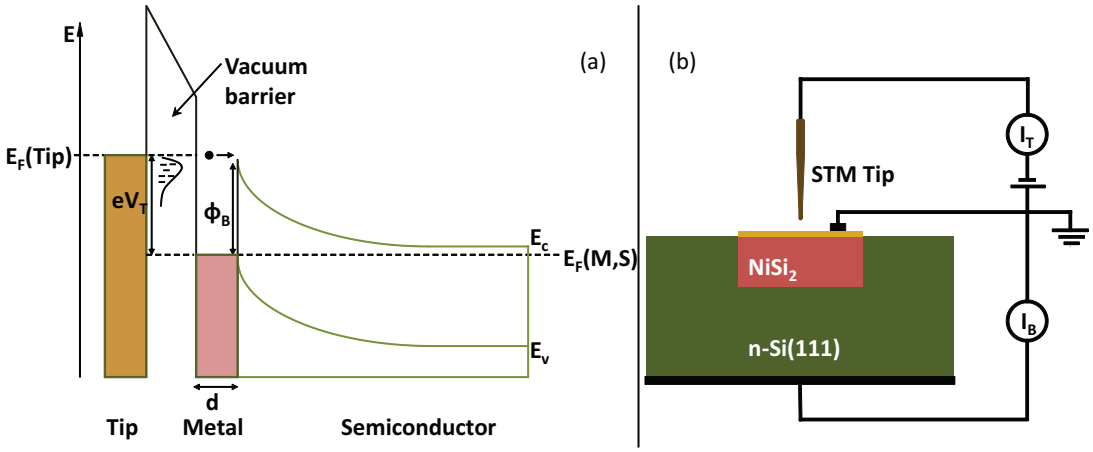

Figure 2.1: (***a***) *Schematic energy representation of BEEM. A fraction of the electrons injected by the tip into the material with a tip bias greater than the Schottky Barrier* Φ_S *will travel across the barrier and will be detected as collector current. The dashed line is the Fermi energy* E_F *of the metal. By changing the thickness d of the metal overlayer, the attenuation length can be obtained. The figure is not on scale.* (***b***) *Schematic representation of* $NiSi_2$*. The electrons are injected with a STM tip in the* $NiSi_2$ *layer. The collected electrons in the n-Si(111) layer are measured in* I_B*.*

tron . Using Matthiessen's rule and incorporating the different scattering processes we can define the hot electron attenuation length λ_a for electrons (energy dependent) as:

$$1/\lambda_a(E) = 1/\lambda_e + 1/\lambda_i(E) \tag{2.1}$$

where λ_e and λ_i are the attenuation lengths due to elastic and inelastic scattering processes respectively. It is possible to extract λ_a from the BEEM transmission which shows a clear exponential dependence on film thickness. One drawback is that the λ_e and λ_i can not be measured directly by BEEM. However, the inelastic attenuation length is energy dependent and proportional to the product of the group velocity and the lifetime, or see eq. 2.2 [7].

$$\lambda_i(E) \propto \sqrt{E + E_F} \times E^{-2} \tag{2.2}$$

The attenuation length is an experimentally obtained number. The BEEM current is a product of the transmissivities through the metal overlayer, the interface and semiconductor. Under the same tunneling conditions, the electrons injected into the metal overlayer with energy E will decay exponentially with the base thickness d. This results in the following expression:

$$I_B(E,T,d) = I_T A(E) B(E,T) \exp\left[\frac{-d}{\lambda_a(E,T)}\cos(\theta)\right] \tag{2.3}$$

Here is $A(E)$ the kinematic transmission factor for electron transport from the metal to the semiconductor, $B(E,T)$ is the transmission factor for electron transport through the semiconductor, I_T the injected current and $\cos(\theta)$ the angle between the injection

tip and the surface normal [8].

In this case the tip is always perpendicular to the surface and by keeping the temperature T and the semiconductor the same, 2.3 is simplified to 2.4.

$$I_B(E, D) = I_T * Const * \exp\left[\frac{-d}{\lambda_a(E)}\right] \tag{2.4}$$

By comparing BEEM spectra, where the fraction I_B/I_T can be obtained, for samples of different thicknesses the attenuation length $\lambda_a(E)$ can be obtained.

2.1.2 BEEM spectroscopy

One of the modes to use the BEEM system is the spectroscopy mode. The spectroscopy measurement can be obtained by sweeping the tip bias, V_T, and measuring the BEEM current when the tunnel current, I_T, is kept fixed. This can be plotted in a I_B vs V_T, where I_B has to be normalized by I_T, because I_B is I_T dependent as can be seen in equation 2.3. At low bias voltages the BEEM current will be zero, since the electrons do not have enough energy to cross the Schottky Barrier. As the voltage is increased the electrons will at some point be collected, as they now can cross the SB. This voltage is the threshold voltage (V_0), which corresponds to the onset of the BEEM current.

The SBH can also be extracted from the BEEM measurement. Following the Bell-Kaiser theory [3], the collector current can be written as equation 2.5.

$$I_C = R \int_{E_x^{min}}^{\infty} dE_x D(E_x) \int_0^{E_t^{max}} dE_t [f(E) - f(E + eV)] \tag{2.5}$$

R is a measure of attenuation of scattering in the base layer and interface, this R is bias independent. The Fermi function $f(E)$ is defined as $f(E) = \{1 + \exp[(E - E_F)/kT]\}^{-1}$. Evaluating equation 2.5, the leading-order term is proportional to $(V - \Phi_B)^2$, because both E_x and E_t are proportional to the $(V - \Phi_B)$ term. Close to the threshold, this model will yield a parabolic shape for the I_C-V spectrum. So equation 2.5 will simplify to equation 2.6.

$$\frac{I_C}{I_T} \propto (V_T - \Phi_B)^2 \tag{2.6}$$

Taking the root of both sides equation 2.7 is obtained.

$$\sqrt{\frac{I_C}{I_T}} \propto (V_T - \Phi_B) \tag{2.7}$$

Making a plot of equation 2.7, the Schottky Barrier Height Φ_B can be determined by the intersection of the y=0 axis and a fit of the linear part of the graph.

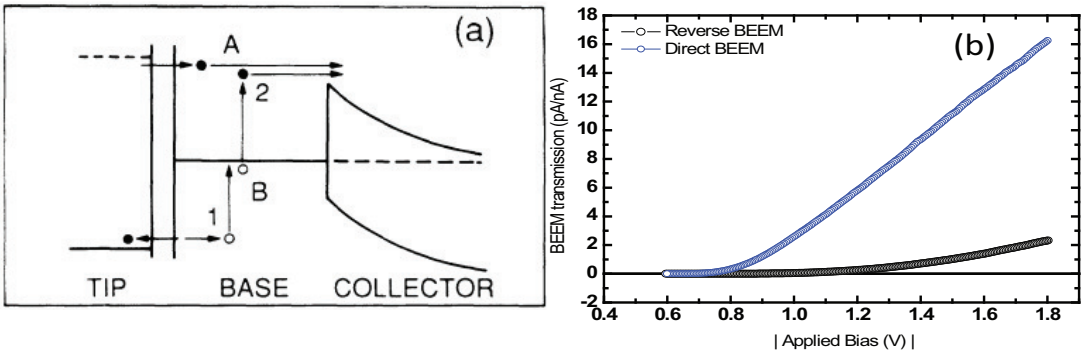

Figure 2.2: (***a***) *Schematic Energy drawing of the Reverse BEEM. In A is the forward BEEM represented, in B the reverse BEEM. In (I) a hole-electron distribution takes place. In (II) the holes scatter with equilibrium electrons, which are collected [9].* (***b***) *BEEM transmission graphs with forward and reverse BEEM of the same sample, the transmission spectra of forward BEEM are always higher than reverse BEEM. In this case the direct BEEM is approximately 8 times the reverse BEEM.*

2.1.3 Reverse BEEM

Instead of injecting and probing hot electron in the metal base, it is also possible to probe hole transport through materials. This provides a direct spectroscopy of electron and hole scattering. By using a positive tip bias, holes are injected into the metal, which then inelastically scatter with the equilibrium electrons, producing electron-hole pairs. The electrons thus created are collected in the semiconductor. This phenomena is known as the reverse BEEM. Only electrons with energy $-V_T > \Phi_B$ and with the right phase space requirements can be collected. This will result in a spectrum with threshold $(V_T - \Phi_B)^4$ [3, 9]. So the SBH can also be derived from reverse BEEM, by making use of equation 2.8.

$$\sqrt[4]{\frac{I_B}{I_T}} \propto (V_T - \Phi_B) \tag{2.8}$$

2.1.4 Formation and macroscopic characterization of a Schottky Barrier

When a metal and a semiconductor are brought in contact with each other, a Schottky Barrier (SB) is formed. Electrical transport across such a Schottky barrier, from where charge carriers are depleted, can be described by the thermionic emission theory where the majority carriers move over this potential barrier. The magnitude of the Schottky Barrier Height (SBH) is the mismatch in the energy of the majority carrier band edge of the semiconductor and the metal Fermi level across the Metal-Semiconductor interface [10].

This SBH can be measured in a I-V relation. Equation (2.9) shows the net current density, with Φ_B the SBH, n the ideality factor and V_a the applied bias.

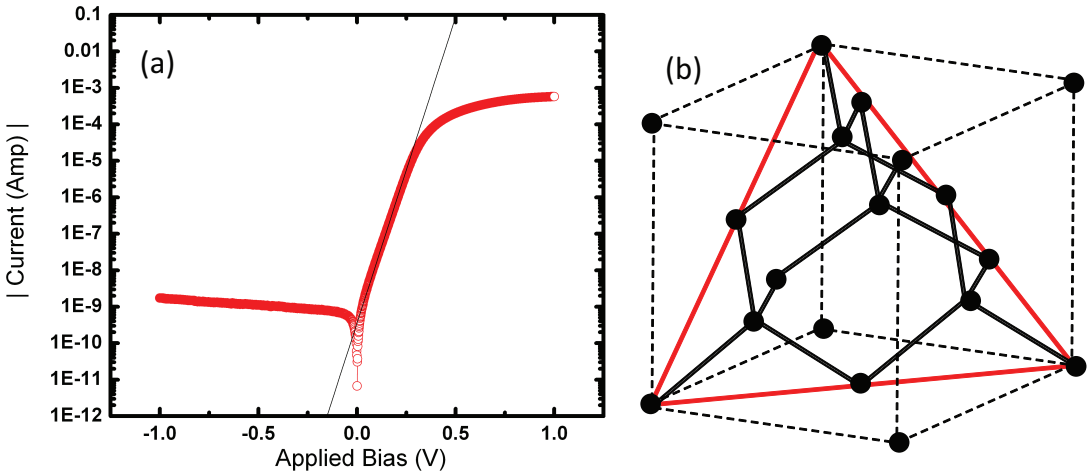

Figure 2.3: (***a***) *I-V relation in a Schottky Diode, a negative bias is the reverse direction. The slope of the graph in the positive bias can be used to determine the SBH. In this case the Schottky Barrier Height of Al on Si(111) is equal to 0.73 eV.* (***b***) *Si has a diamond crystal lattice structure. The red line shows the (111) plane.*

$$J = A^* T^2 \exp\left(\frac{-e\,\Phi_B}{kT}\right)\left(\exp\left(\frac{eV_a}{n\,kT}\right) - 1\right) \tag{2.9}$$

Here is A^* the effective Richardson constant, see equation (2.10). For n-type Si this constant has a value of 110 A cm^{-2} K^{-2} [11].

$$A^* = \frac{4\pi e m_n^* k^2}{h^3} \tag{2.10}$$

The net current density depends on the temperature T, the applied voltage V and the Schottky Barrier Φ_B, depending on the material. This SB does not change in one sample, so when T is held constant, the current can be measured when the applied voltage is measured. Plotting the I-V relation of a Schottky Diode, a graph like figure 2.3a can be obtained. The linear portion can be used to determine the SBH. The black line is equation (2.9) plotted in the graph. The value of the Schottky Barrier Height obtained from I-V measurements represents an average barrier height at the M-S interface whereas BEEM spectroscopy measurements can give us information about Schottky Barrier Height inhomogeneities at the nanoscale.

2.2 Formation of epitaxial $NiSi_2$ on chemically treated Si(111) substrate

Silicon has a diamond crystal lattice structure. Si(111) is the way to denote in which direction the silicon grows. This distinguishes Si(111) from Si(100). The (111) crystal plane is shown in figure 2.3b. $NiSi_2$ grows epitaxially on Si(111) plane with a lattice mismatch of 0.46%. Thus a careful preparation of Si(111) plane is essential for the epitaxial growth for $NiSi_2$ for our studies.

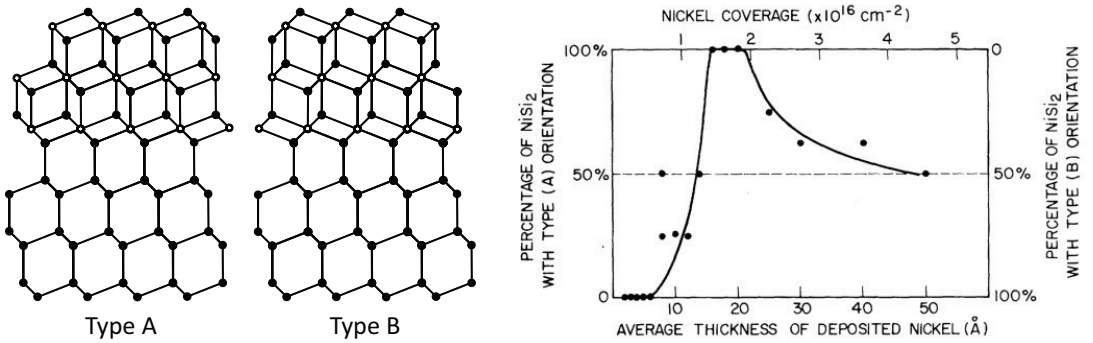

Figure 2.4: (***a***) *Balls and sticks models of the two $NiSi_2$-Si(111) interfaces viewed in the* $\langle 1\bar{1}0 \rangle$ *direction. Black balls are Si, white are Ni atoms [18].* (***b***) *The percentage of $NiSi_2$ volume with type-A and type-B orientation is dependent on the average thickness of deposited nickel [19].*

The preparation of a smooth, clean and undamaged surface is important for many fundamental and technical processes. Etching silicon can produce very flat hydrogen terminated surfaces. A wet chemical method using 40%NH_4F is a known and established technique to produce these Si(111) surfaces [12]. There are different parameters which contribute to a high-quality Si-surface: the cleanliness of the wafer, the situation of the oxide layer, the evolution of cleanliness during etching and the influence of dissolved O_2 in the etching solution [13]. The oxide layer removal was already optimized by using 8 min 30 s BHF. 1 m%HF is used for hydrogen-terminated silicon surface, leaving the surface silicon atoms covalently bonded to hydrogen. In this experiment the parameters for the time to remove the dissolved oxygen (by bubbling N_2 in the solution) and the etching time in NH_4F are investigated and optimized in order to create flat surfaces which can be used later on as a substrate for spin-valves. NH_4F attacks bulk silicon anisotropically which etches Si(100) faster than Si(111) and should result in the formation of Si(111) [14]. There are several studies to search for optimized chemical treatment to create flat Si(111)-surfaces, which can be terraces or pillars, but the articles contradict each other [12, 15–17], there are differences from substrate to substrate. So to create flat hydrogen-terminated Si(111)-surfaces with our substrates, different etching and bubbling times were used to optimize the process, see section 3.1.

2.2.1 $NiSi_2$

Thin films of single-crystal $NiSi_2$ can be grown with very high degree of perfection on silicon [19]. $NiSi_2$ has good electrical properties as well as unique structural characteristics [20]. Disilicides of Ni are ideal choice for the epitaxial growth as they have the cubic CaF_2 structure and with a lattice match within 1.2% of Si [21]. The $NiSi_2$ films can be grown on Si(111) along the same surface normal $\langle 111 \rangle$ and either with the same orientation to that of the substrate (Type A) or rotated 180° about the surface-normal direction (type B) [19, 22], see figure 2.4a. The SBH has a different value for the A-type and B-type, namely 0.65 eV and 0.79 eV respectively [18]. The favored orientation is dependent on the average thickness of the deposited nickel on

the Si-surface, as can be seen in 2.4b. Thin layers of 1-7 Å Ni are Type-B oriented and those with 16-20 Å of Ni are type-A oriented. So far, no work exists on the study of hot electron attenuation length of $NiSi_2$ on n-Si(111). This is important in our case as we have already used such epitaxial interfaces for fabricating metallic spin valves and studying spin transport properties across such epitaxial M-S interfaces. Thus quantifying the attenuation length in $NiSi_2$ and understanding the underlying scattering processes in such M-S epitaxial interfaces is relevant and interesting.

$CoSi_2$ is another class of epitaxial silicides which has been well studied. The lattice mismatch with the underlying Si substrate is larger than that in $NiSi_2$. Attenuation length of $CoSi_2$ on n-Si(111) has been studied by Lee *et al.* [6]. They found the attenuation length λ to be 40 Å at 3 eV.

Chapter 3

Experimental

3.1 Chemical treatment of Si(111)

In order to investigate the Si(111) morphology produced by wet chemical etching in 40%NH_4F with different bubbling times and dipping times, we adapted a protocol based on the method of Higashi [12]. The as-received Si wafers have in general a thick SiO_2 layer, protected by a layer of photoresist. These layers have to be removed in order to reach the Si. All the following steps were done at RT (room temperature).

First a small piece (0.6 mm^2) of n-Si substrate was chosen from a bigger silicon-wafer. Because there were different wafers available and partly processed, the wafers are separated by naming them as 'old' and 'new'. All the starting substrates had a Au-Cr back contact. To remove the photoresist, the samples were cleaned in an ultrasonic acetone bath for 15 minutes. The samples were always clamped in a 4-legged sample holder for all chemical steps. Later on in the experiments the resist-layer was removed by dipping the substrates for 10 m in 100% HNO_3, because HNO_3 removes organic resist and other contaminants as well as inorganic contaminants better. The samples were rinsed with DI water and dried with a N_2-ion dry-pistol; this was done after each step in the process. The oxide layer was removed by dipping in BHF for 8 min 30 s. 1%HF dipping for 60 s was done for hydrogen-termination of the surface. This leads to a passivated and clean Silicon surface. In order to etch the silicon surface with NH_4F, oxygen needs to be removed from the solution. To achieve this, a small tube on a N_2-ion dry-pistol was used to bubble N_2 into the solution. This was done for different times, depending on the experiment. After this bubbling, the sample was dipped in the solution. The NH_4F will remove the Si(100) planes, because the etch rate is higher than that of Si(111). So only Si(111) will remain. After 15, 20 or 30 minutes (depending on the experiment) the sample was removed from the NH_4F solution and rinsed in a beaker of DI water that also had been bubbled with N_2 to remove oxygen. Then the N_2-ion dry-pistol was used to dry the Si(111). There were however problems with bubble formation on the surface due to drying the water with the N_2-gun, see figure 3.1. To solve this, no standing water but flushed water was used after the NH_4F treatment, and a dry-spinner was used to dry the silicon.

After this chemical treatment, the surface morphology and RMS roughness was mea-

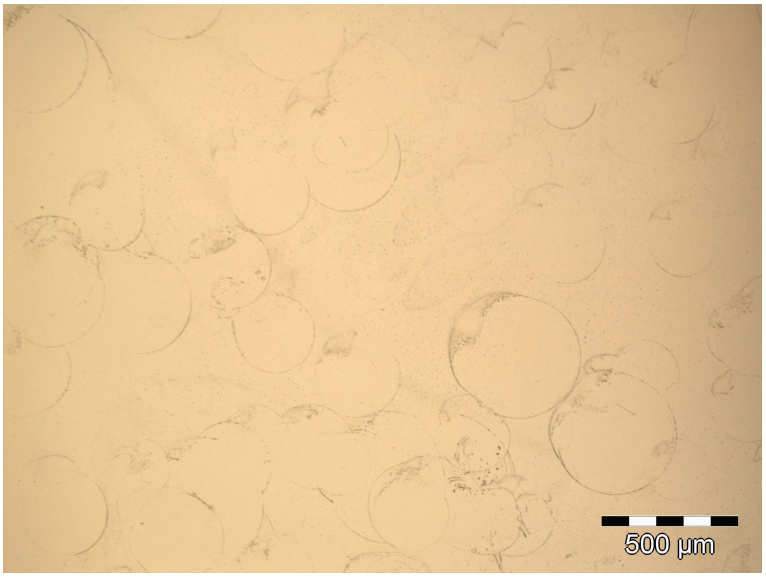

Figure 3.1: *Bubble residue on surfaces can be seen with an optical microscope.*

sured with the AFM. STM measurements were attempted but we were not successful in obtaining a good image.

3.2 Growth of epitaxial $NiSi_2$ on Si(111)

Growing $NiSi_2$ thin films on Si(111) was done in an ultra high vacuum molecular beam epitaxy (UHV MBE) system, based on the method of Tung *et al.* [19]. There are two steps, the surface treatment and the deposition itself, see figure 3.2. In this experiment the 'old' substrates were used, because this process was already used before and optimized. The silicon substrates were prepared in almost the same way as was done with the substrates described in section Si(111) in 3.1. There is one major difference between the chemical treatment steps. This substrate has a resist on top, and a lithographically defined area of 150 μm. Instead of removing the photoresist with HNO_3 first, now the SiO_2 is first removed with BHF (8 min 30 s) and thereafter the photoresist is removed with 10 min HNO_3. The substrate is H-terminated with 1 min 1%HF. After each step the surface was cleaned with DI-water and dried. In this way a Si(111)-surface is surrounded by a thick SiO_2 oxide layer. Now the silicon was etched in 40%NH_4F for 15 min after this was bubbled with N_2 for 20 min. Afterwards, the substrate was dipped in water that was also bubbled with N_2. After each step in the process, the substrate was rinsed with DI-water and dried with the nitrogen-gun. After the chemical treatment, the Si-surface was quickly loaded in the MBE-system.

With the MBE-system the deposition of Ni and the formation of $NiSi_2$ was done. First, the sample was loaded in the load lock of the MBE-system, then a vacuum pump was used to lower the pressure to 10^{-6} mbar. With this pressure the sample could be transferred to the main chamber, which has a pressure of 10^{-10} mbar. In the main chamber the sample was positioned so that the Ni could be deposited from a Knudsen

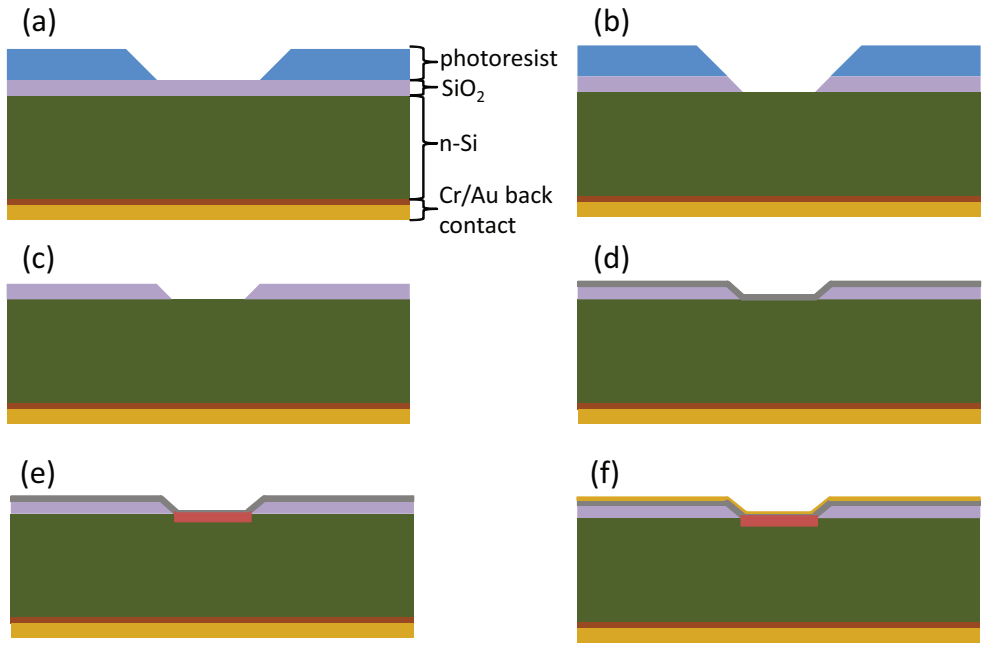

Figure 3.2: *Schematic representation of wet chemical etching and deposition to make the samples (**a**) Standard substrate as delivered. The n-Si is covered with a layer of SiO_2 and photoresist. There is a lithographically patterned area in it. The bottom of the silicon has a Au-Cr back contact. (**b**) BHF to remove SiO_2-layer, this SiO_2 will only be removed on the place where the patterned area is located. It is not possible to etch under the photoresist layer. (**c**) The photoresist is removed with HNO_3. After this step the surface is hydrogen-terminated with HF and etched with 40%NH_4F. (**d**) Deposition of Ni-layer in MBE-system on substrate. (**e**) Annealing the sample to grow $NiSi_2$. The red layer is the $NiSi_2$-layer. (**f**) The substrate is capped with gold.*

cell on the Si-surface. The Ni K-cell was heated to 1440°C for a certain amount of time at RT and this resulted in a thin layer of Ni. The time of deposition was varied so as to obtain different samples with different thicknesses. An earlier calibration with the AFM showed that a 4 min deposition forms a 1 nm Ni-layer. For thicker Ni layers, deposition was done for 4-5 min at RT (∼1 nm) , thereafter the temperature was slightly increased to ∼300°C/400°C to initiate the formation of epitaxial $NiSi_2$ at the interface. Then the rest of the deposition was done. In all cases, to create the $NiSi_2$ layer the temperature needs to be above 500°C for 5 minutes, such that an epitaxial silicide is formed at the interface. The temperature of the substrate was regulated with a power source and monitored with a pyrometer. The thickness of the $NiSi_2$ is approximately 3 to 3.5 times the deposited Ni layer thickness [23]. For this experiment the value 3 is used. The device was then covered with an Au cap layer at RT, evaporated from a Au K-cell. A 4 nm thick Au-cap was deposited from a K-cell heated to 1305°C, achieved after a 20 min deposition. This device was then removed from the MBE-system and loaded into an UHV STM, so BEEM measurements could be performed. The setup for this experiment is shown in figure 2.1b.

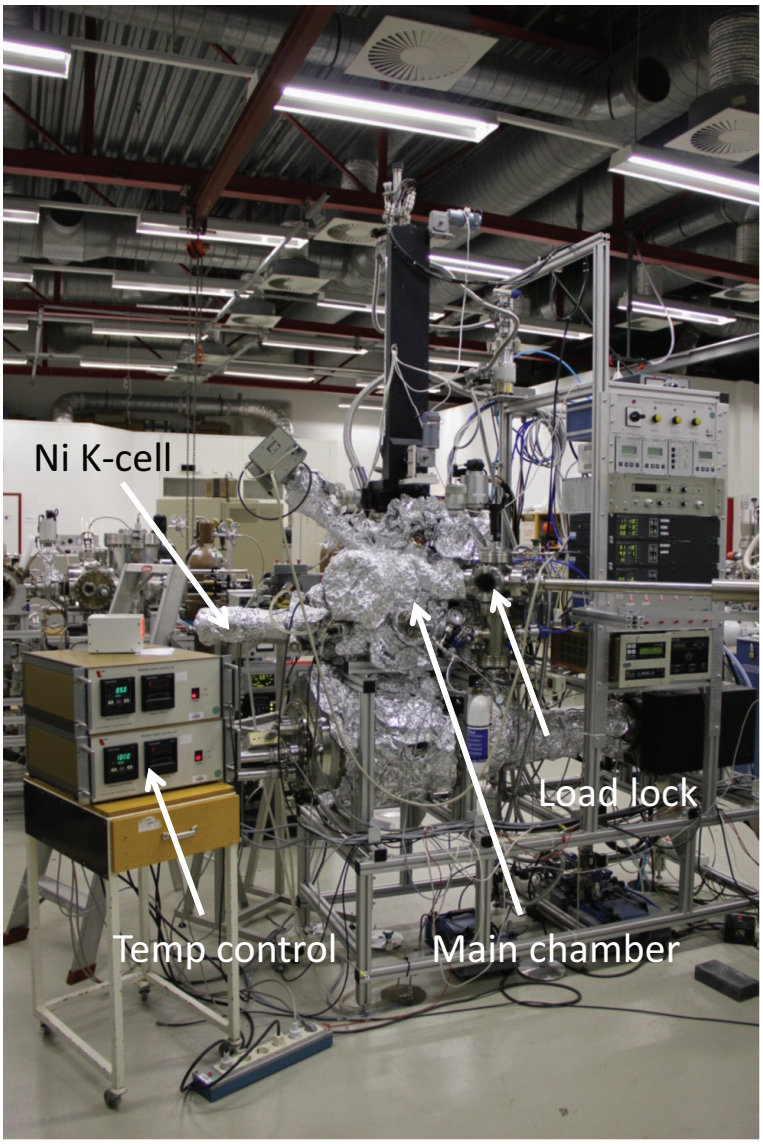

Figure 3.3: *MBE system.*

3.3 Experimental set up: BEEM

The experiments were done in a commercial BEEM setup from RHK, at an ultra high vacuum of 10^{-10} mbar. Also the temperature and the magnetic field can be controlled. The system can be cooled by using liquid nitrogen. The BEEM system is placed on a table with air legs to decrease vibrations. Inside the BEEM there are two vacuum chambers, the main chamber where the measurements take place and the load lock to insert the sample. A rotary and turbo molecular pump are used to get a pressure of at least $5x10^{-6}$ mbar, the main chamber has a pressure around 10^{-10} mbar maintained by a ion pump. A transfer arm is used to transfer samples from the load lock to the main chamber and back. A wobble stick is used in the main chamber to position the sample.

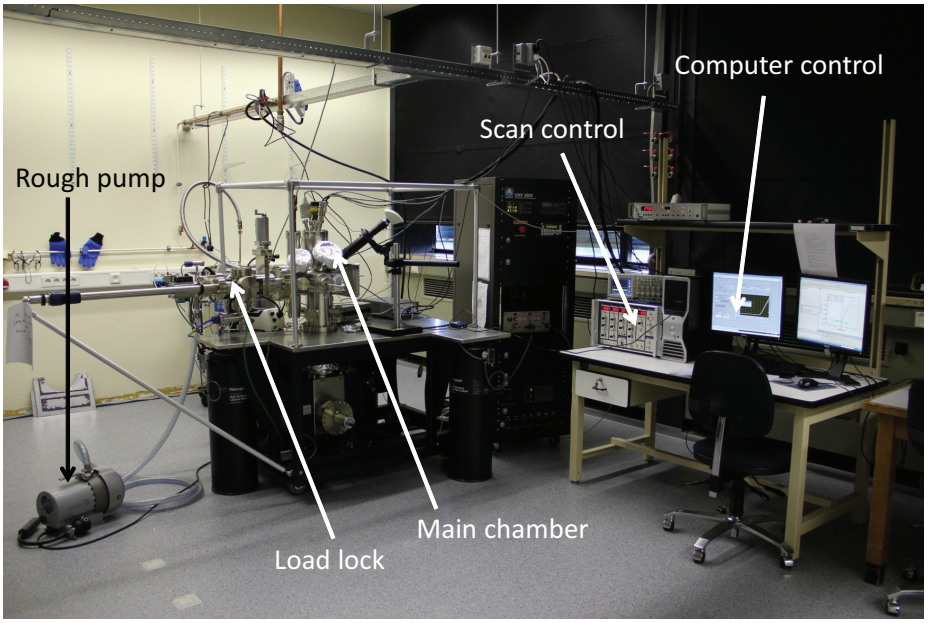

Figure 3.4: *BEEM system.*

The $NiSi_2$ samples were placed on a sample holder after deposition in the MBE system. This sample is used to collect the BEEM current. The sample itself is placed in a copper basket on which a sapphire washer is place to ensure that there is no electrical contact. Gold contacts ground the top metallic surface, as can be seen in figure 2.1b. After the sample was placed on the sample holder, the sample holder was placed in the load lock of the BEEM system.

After pumping and transferring the sample to the main chamber, the sample was cooled using liquid nitrogen. The temperature inside the main chamber is higher than the boiling point of nitrogen (77 K), -somewhere around 100 K. When the temperature was stabilized, the measurement could begin, otherwise the tip will drift due to temperature fluctuations. First, a 2-probe measurement was performed so the macroscopic SBH could be determined. The 2-probe was performed with a Keithley 2400 and a LabView program which could sweep the voltage and measure the current. The voltage sweep was between -1 and 1 V. The LabView was made in an earlier small internship ('FIT-stage'). Then the BEEM spectroscopy was performed. To do this, the tip was lowered until a good tunnel current was achieved. The tunnel current was set at 1 nA for the direct BEEM and 3 nA for the reverse BEEM. Then a voltage sweep was performed, while holding the tip at a constant height, ranging from -2.0 V to -0.6 V. To measure the BEEM current (I_C) a two stage amplifier SR570 from Stanford Research with an overall gain of either 10^{10} or 10^{11}V A-1 is used. In most cases the gain used was 10^{10} so that means that 1 V corresponds to 10 pA. After the voltage sweep was done, the voltage is set back to -2.0 V and the measurement was done again. After 10 measurement, the average was taken. The measurements were done at different locations on the substrate, so the BEEM transmission could be calculated from more than one hundred BEEM spectra.

Chapter 4

Measurements

In this measurement chapter two separate topics are discussed. First, the preparation of Si(111) surfaces is described and investigated with AFM. Then the topic changes to the investigation of transport across epitaxial $NiSi_2$/Si(111) interfaces. The BEEM spectra are shown and the hot electron attenuation length is extracted. Two important parameters experminted with are the *dipping* time and *bubbling* time. The dipping time is the time that the sample is in contact with the chemicals. The bubbling time is the time that the N_2-gun was used to blow nitrogen into the solution to remove the dissolved oxygen. See for further details section 3.1.

4.1 The preparation of flat Si(111) substrates

Already a lot is investigated and reported in the literature about the preparation of passivated Si(111) surfaces. Suzuki and Adachi [24] found something interesting. They found that the etching of Si(111) surface in NH_4F solution is not uniform. Immersing the silicon sample for a longer time causes the sample surface to be rougher in a solution with oxygen. Ouayang *et al.* [25] also saw large fluctuations in their experiments. Bubbling nitrogen in the solution showed that the RMS roughness decreased, but also the etch rate. They also observed that the etching of Si(111) almost stops in the oxygen-free solution. Dissolved oxygen initiates formation of etch pits on Si-surfaces.

4.1.1 Optimization of parameters for flat 'new' Si(111) substrate

The first experiment that was performed was by changing the bubbling time and dipping time for the new substrate. For the old substrate, the optimized time for bubbling was 20 min; for dipping 15 min. In this case the experiment was performed in the following way: The sample was cut in two, after 10 min HNO_3 and 8 min 30 s BHF treatment, the samples were dipped in 40%NH_4F that had been bubbled for 30 min. One of the samples was removed after 15 min, the other after 30 min. This experiment was repeated, but now with the bubbling time increased to 1 hour. There was gas formation on the surface, this was not the case with the old substrates. The results of the AFM can be found in figure 4.1a-d. In figure 4.1a, it can be clearly seen that there is pillar formation. The figures 4.1b-d show a complete different surface morphology,

i.e. no pillars at all. The structure almost looks like after only the HF treatment. The roughness for the images b-d is around the 2 Å, the pillar formed structure shows only this value in very small areas, in the complete picture this value is around 1 nm. A longer bubbling time removed the pillared structure, as can be seen from 4.1a and c. Only one article so far discussed the pillars as due to DO [15]. In this case there also gas formation on the surface was observed. What the problem could be is that the oxygen is not properly removed from the solution, which will result in the formation of pillars at 30 min bubbling. Althought 60 min bubbling doens't show terraces, the RMS roughness is considerably lower.

Comparing our AFM images and RMS roughness results with literature, there seems to be an agreement. If the surface is, in our case, very rough with a bubbling time of 30 min, probably the oxygen is still not removed from the solution. The 60 min bubbling shows however a flatter surface. So probably the oxygen is not removed at short times and it needs longer bubbling time. However the optimum parameters are not yet found. Another way to create an oxygen-free solution is by using 0.5% $(NH_4)_2SO_3$ as Kato *et al.* suggest [13]. However, this idea was not checked in our case.

The lower roughness with a longer dipping time is harder to explain. One would expect that the surface becomes rougher, because the surface is longer exposed to etching. Probably the etching rate is very low [25], so the roughness is very low. Kato found an optimized time of only 10 minutes etching, so 15 min and 30 min are on the high side.

Also some other experiments were performed on the new substrate to search for a flat silicon surface. These can be found in figure 4.1e-g. Figure 4.1e is the experiment were no HF and no bubbling was done, but only a dip of 1 min 45 s in 40%NH_4F. This surface roughness was between 6 and 10 Å. This is thus a solution with O_2, which results in a high RMS roughness. In figure 4.1f the surface without HF, but with 5 min prebubbling and 4 min dipping and bubbling. Bubbling while dipping was done, to prevent hydrogen formation on the surface. This surface is rather flat, between 3 and 6 Å. The most remarkable thing are the holes in substrates. The holes are formations of etch pitches as a result of still dissolved oxygen in the solution. Figure 4.1g shows a very rough surface, this was created by no HF and 10 min dipping and bubbling. The roughness is around the 1.3 nm. The reason why there is a huge difference in surface morphology between figures 4.1f and g, although the total N_2 time is approximately equal, has something to do with the prebubbling. The latter substrate is immersed in a solution which contains a lot of oxygen, whereas the first substrate is dipped in the solution, where already oxygen was partially removed with (pre-)bubbling. As said before, etching in a solution with oxygen in it, will cause a rough surface. The last picture in figure 4.1h, shows the surface after 20 min bubbling and 15 min dipping. These values were optimized for the old substrates, but it can clearly be seen that it doesn't work for the new substrate. This surface is not comparable with any of the other pictures.

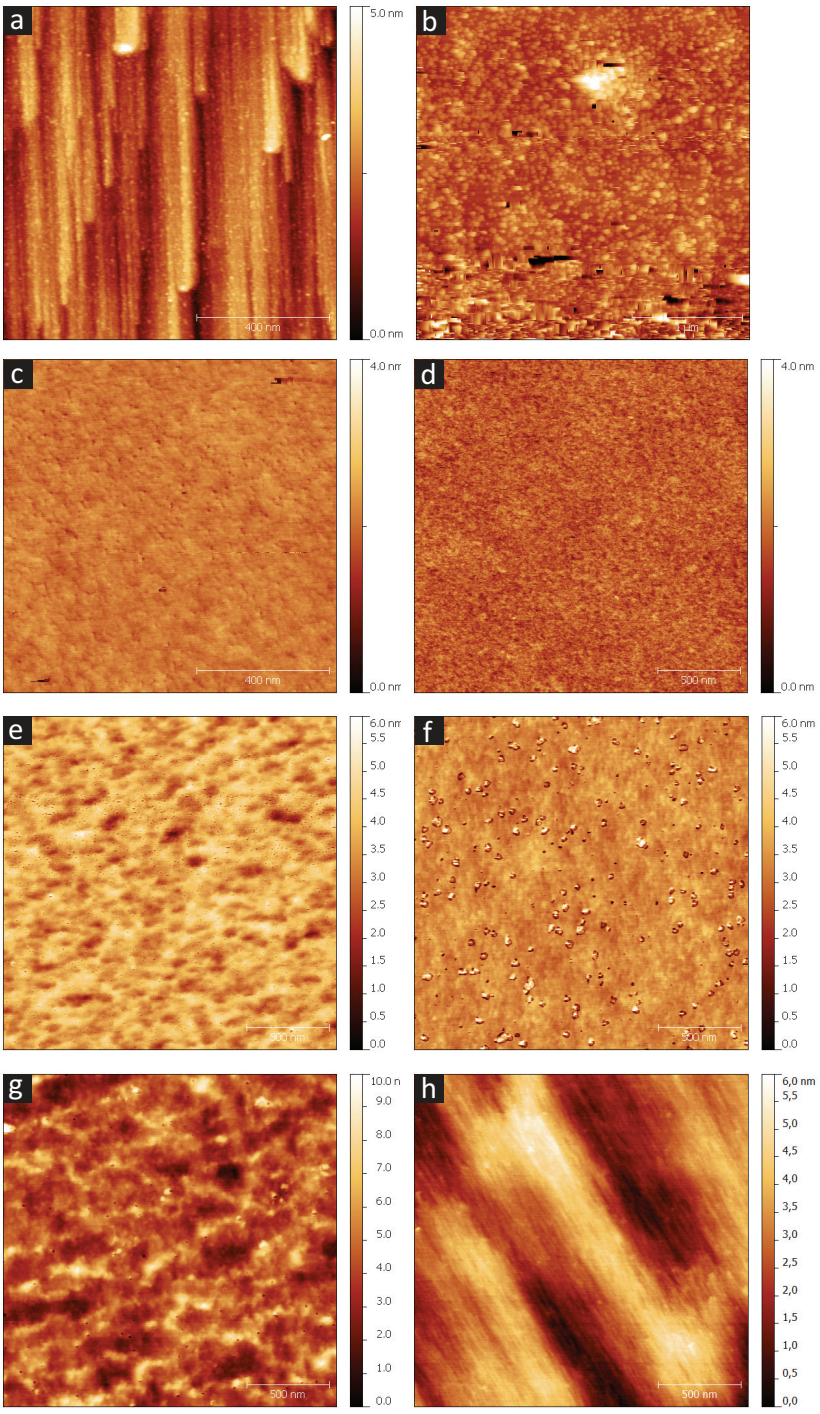

Figure 4.1: *AFM images, (1×1) µm for a-d and (1×1) µm for e-h, of silicon substrates after wet chemical etch (**a**) Bubbling for 30 min, dipping 15 min. (**b**) Bubbling for 30 min, dipping 30 min. (**c**) Bubbling for 60 min, dipping 15 min. (**d**) Bubbling for 60 min, dipping 30 min. (**e**) No HF, no bubbling, 1m45s dip in 40%NH_4F. (**f**) 5 min bubbling, thereafter 4 min dipping in 40%NH_4F with bubbling at the same time. (**g**) 10 min in dip 40%NH_4F with bubbling at the same time. (**h**) 20 min bubbling and 15 min dipping. These parameters were the optimized ones for the chemical treatment for the old substrate.*

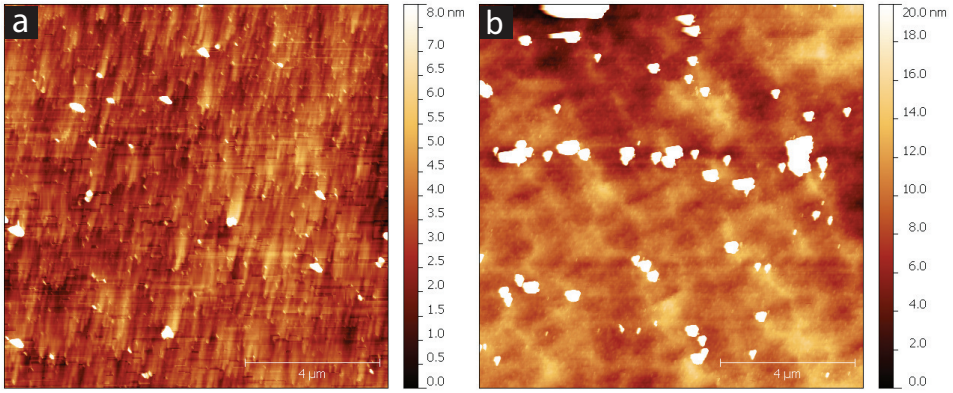

Figure 4.2: *AFM images showing difference between the old and new substrate. The chemical treatment on the substrates was done at the same time and with the same procedure. 10 min HNO_3, 10 min BHF, 1 min HF, 20 min bubbling and 23 min dipping in 40%NH_4F. Images are (10×10 µm) (**a**) is the old substrate, (**b**) is the new substrate. The quality of the AFM images is not very good.*

4.1.2 Difference old and new substrate

In figure 4.2 the difference between the old and the new substrate can be seen clearly. Both substrates were equal in size and the parameters of the wet chemical etch were the same. The chemical treatment was done at the same time, so there is no difference in the parameters, except for the substrates itself. In fig. 4.2a the formation of pillars can be seen, whereas in fig. 4.2b a rougher surface can be seen. The RMS are 0.91 and 2.2 nm respectively. Also the RMS roughness of smaller areas were measured, as for BEEM only smaller areas are used. Then the RMS values are: 0.50 ± 0.12 and 1.25 ± 0.58 nm respectively. In this case the average of multiple areas was taken. A clear evidence of a difference from substrate to substrate can be seen.

4.1.3 The chemical treatment step by step

A part of the experiments with the Si-substrates was to see what happens with the surface after each step in the chemical treatment. If the surface is not flat enough in the beginning, then it will never become flat in the rest of the process. For this experiment the old substrate is used. After each step in the process an image with the optical microscope was taken and AFM images were obtained. Multiple AFM images were taken, both large and small areas, but not all images are shown. Afterwards, the next step in the process was done followed by imaging, etc. The results can be seen in pictures 4.3 and 4.4.

The Si-surface as it is on the wafer can be seen in figure 4.3a. Then the first step was done: 10 min HNO_3 to remove the photoresist. Here only an optical microscope image was taken and can be seen in figure 4.3b. This was followed by 8 min 30 sec BHF to remove the SiO_2. Results are shown in 4.3c and 4.4a-b. In figure 4.4a the large area scan of 15x15 μm can be seen where some islands are located. These islands are probably not removed residues of SiO_2. In the following steps, the islands are not

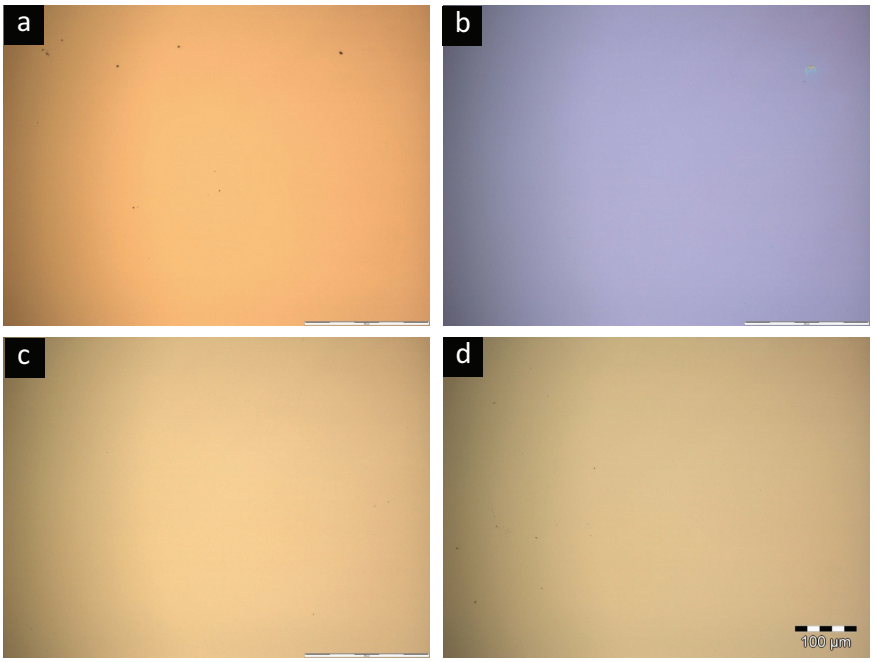

Figure 4.3: *Optical microscope images after the different steps in the chemical treatment process. The scale bar of the first three images is 200 µm.* (***a***) *Si(111) + SiO_2 + photoresist. This is the standard substrate from the wafer.* (***b***) *Si(111) + SiO_2. The substrate is dipped in HNO_3.* (***c***) *Si(111). The oxide layer is removed with BHF.* (***d***) *Si(111). After the BHF and in addition 1m 1%HF H-termination.*

removed and on all large area AFM images these can be seen. During BEEM measurements one can selectively choose the areas where there are no islands. An image of 1x1 μm is seen in 4.4b, it shows a very flat surface, with an RMS roughness of $\sim$1 Å.

The next step is the hydrogen termination using 1%HF for 1 min. The results are shown in figures 4.3d and 4.4c. Also in this case the surface is very flat in the small area scan, the RMS roughness is here again around 1 Å. So the HF has no influence on the roughness and morphology of the surface.

The final step is the bubbling with N_2 and 40%NH_4F. The times used in this case are 20 min bubbling and 15 min dipping. The AFM image can be seen in figure 4.4d, however an optical microscope image was not taken, because the AFM imaging had to be done quickly, otherwise the substrate would oxidize. The most remarkable thing that can be observed is, of couse, that the substrate is not as flat as before (compared with the other images). The RMS roughness was now approximatly $\sim$5 Å, almost 5 times higher than before this etching step. So the step that contributes to the high RMS roughness is the etching in NH_4F. This fact might also be an indication that the oxygen is not fully removed from the solution yet. A high RMS roughness indicates that there is a high etching rate, but Ouyang [25] found that only in an oxygen environment there is an high etching rate. The biggest problem, however, is that the reproducibility is gone. Images 4.4d and 4.2a are the same substrate, with the same wet chemical etching, but they show complete different surface morphology. There are

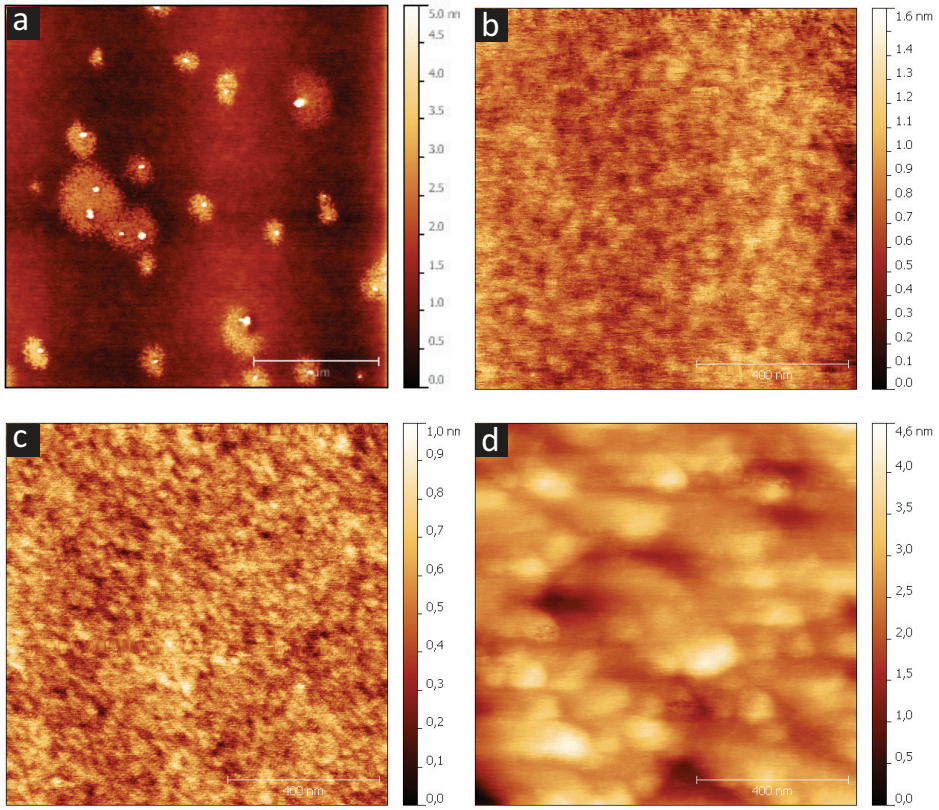

Figure 4.4: *AFM images of Si(111) substrates. Last three images are 1×1 μm* (***a***) *Large area scan, after 10 min HNO_3 an 8 min 30 sec BHF. SiO_2 can clearly be seen on surface.* (***b***) *small area scan of Si(111), zoomed in on (a).* (***c***) *After additional 1%HF step for 1 min.* (***d***) *Si(111) after final 20 min bubbling and 15 min dipping in 40%NH_4F.*

some flat spots on the substrate (around 2 Å), that could be used for $NiSi_2$ growth and BEEM measurements.

Although the best optimization is not found for the new substrate, it is shown that the current chemical treatment is not the optimum, because of the relatively high surface roughness. This optimization is still under construction and the measurements are not sufficient to do any statistics. The old substrates were used to grow epitaxially $NiSi_2$ on top of it. The surface is not uniformly flat, only in small areas. Longer bubbling might decrease the roughness, but it can be too costly. It was showed that the surface morphology after etching is surface dependent.

4.2 BEEM transmission in $NiSi_2$/Si(111) for different thickness $NiSi_2$

Although the hot electron attenuation length of $NiSi_2$ is not reported so far, a lot of other information can be found about hot electron transmission in $NiSi_2$. Tung did a lot of research on $NiSi_2$/Si formation and properties [19, 22, 23]. He described the formation of $NiSi_2$ on Si(111), which was used in this experiment. The attenuation length of different materials, for example Ag, Au, $CoSi_2$ and Cu, is already researched [6–8, 26]. The experiments were always derived from BEEM transmissions with different thicknesses of materials, accompanied with modeling to extract values for the inelastic and elastic scattering lengths at different energies.

In this section the electronic properties of $NiSi_2$ will be discussed. The direct and reverse BEEM spectra of the different samples, with varying thicknesses of $NiSi_2$, will be discussed. To check whether every time the same sort (type A) of sample was measured, the SBH was measured with the Bell-Kaiser theory, see Eq. 2.7. If the SBH do not change between the samples, then the type of the $NiSi_2$ doesn't change.

The BEEM spectra of different samples were taken. The different thicknesses of $NiSi_2$ were dependent on the thickness of the deposited Ni layer in the MBE. The BEEM spectra were obtained from different areas on the sample. Measurements of the same sample were done for many times, so a reliable average could be taken. The data analysis was done very carefully. The $NiSi_2$-layer has a gold cap on top the so the SBH is not 0.65 eV (type-A for our devices), but it will change. This is probably due to Fermi Level pinning. The measurements were done at low temperature (LT). In each of the following sections the BEEM transmissions are discussed for the direct and reverse BEEM. The only parameter that could be used to control the $NiSi_2$ layer thickness was the time of Ni deposition. Therefore a conversion between these need to be made. 4 min of Ni deposition will result in a layer of 1 nm, this layer then forms a $\sim$3 times thicker $NiSi_2$ layer. The times of the Ni deposition used in these measurements are presented in table 4.1. Because this conversion is only based on previous results and literature and the real thickness could not be checked with these samples, there might be an error of 10% in the calculated thickness.

Deposition time Ni (min)	Thickness Ni layer (nm)	Thickness $NiSi_2$ layer (nm)
5	1.25	3.75
10	2.5	7.5
15	3.75	11.25
20	5	15
30	7.5	22.5

Table 4.1: *Conversion between Ni deposition time and thickness of $NiSi_2$. A 4 min deposition of Ni will result in a 1 nm thick Ni layer. Growing $NiSi_2$ will result in a layer of $\sim$3 times the Ni layer.*

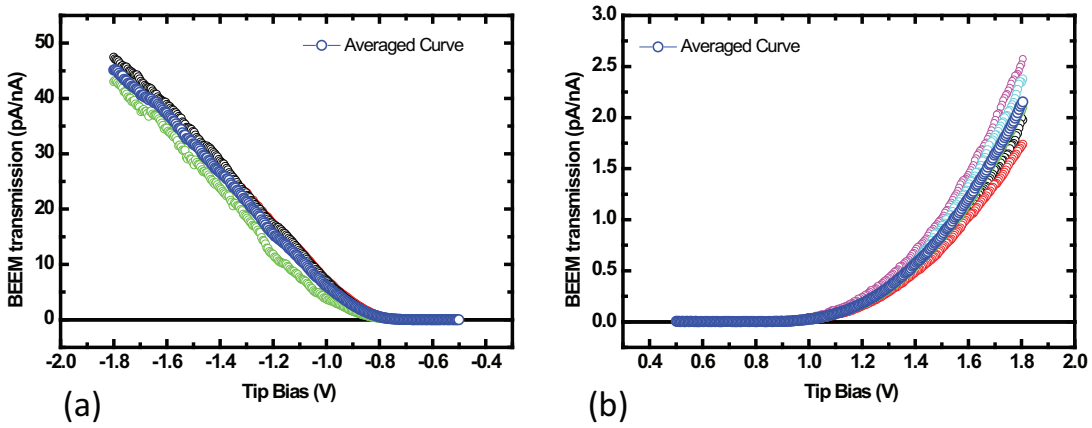

Figure 4.5: *The transmissions for the 5 min Ni deposition for* (***a***) *the direct BEEM and* (***b***) *the reverse BEEM. The average is the blue curve.*

4.2.1 5 min Ni deposition

The 5 minutes of Ni ($\approx$ 1.25 nm Ni and 3.75 nm $NiSi_2$) deposition was not done during this experiment. This data point was taken from an earlier experiment. All devices were fabricated from the same substrate with the same chemical processing, the conditions of the deposition and the experiments in the BEEM were the same as the other samples. The SBH is 0.72 $\pm$ 0.01 eV. Later on, the reverse BEEM was performed on this sample, because these data were not taken earlier. First, the direct BEEM was checked and the spectra showed no variation in transmission compared with the first measurement, which is an indication that the sample is not oxidized. Both measurements showed an average value of 43 pA/nA at a bias of -1.8 V, see Fig. 4.5a. The reverse BEEM, see fig. 4.5b, was very stable, in fact all the reverse BEEM spectra were very stable, as compared with direct BEEM. The difference between the forward and reverse BEEM is in this case a factor 20 at a bias of -1.8 V and 1.8 V respectively.

4.2.2 10 min Ni deposition

The deposition of Ni will result in a layer $NiSi_2$ of approximately 7.5 nm. The plots of the BEEM transmissions can be seen in figure 4.6. Two regions of transmission were clearly visible, as can be seen in fig. 4.7a. Here a separate average of transmissions around 20 and 40 pA/nA were taken. The higher transmission is almost twice as large as the lower one (42 vs 20 pA/nA). To confirm that the difference in transmission is not due to the formation of different types of $NiSi_2$, the SBH was extracted using Bell-Kaiser model, all spectra showed the same SBH of 0.72 $\pm$ 0.01 eV as can be seen in (b). This indicates that the same type of $NiSi_2$, but local areas with $NiSi_2$ have different thicknesses. The SBH at room temperature is also measured with the 2-probe technique and is found to be 0.71 $\pm$ 0.01 eV, which matches with the SBH that was found with the BEEM spectroscopy, see fig. 4.8. Although there were difference in transmission, an overall average was taken to calculate the attenuation length later on. It can not be seen whether one spectra is better than another, so all spectra were taken in the average. The average shows a value of around 30 pA/nA at -1.8 V. None

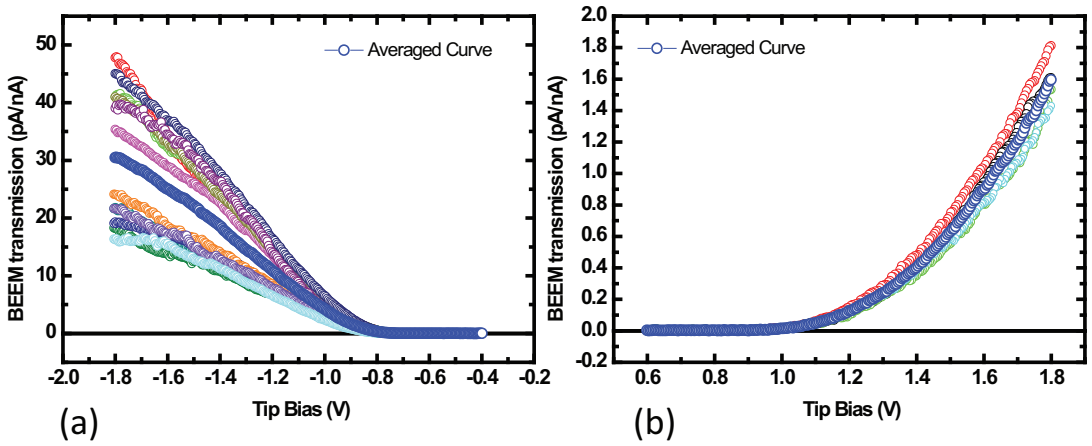

Figure 4.6: (***a***) *All Direct BEEM spectra for 10 min Ni deposition in one plot. The pink line is the average.* (***b***) *All Reverse BEEM spectra for 10 min Ni deposition in one plot. Again, the blue line is the average of all spectra.*

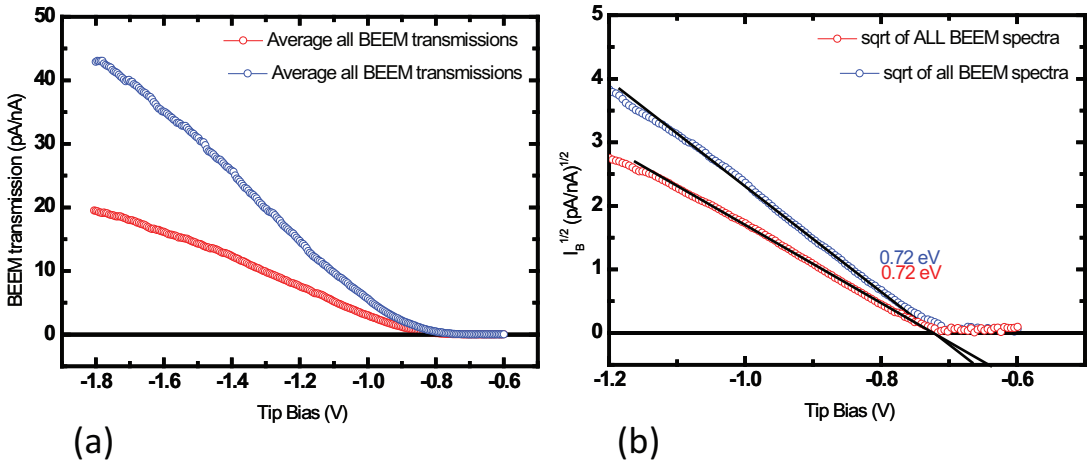

Figure 4.7: (***a***) *BEEM transmission versus Tip Bias shows two different slopes. The slopes differ approximately two times.* (***b***) *The sqrt of the BEEM current versus the Tip Bias. The black line is the fitting of the linear part of the slope. The SHB of the two curves (from (a)) show the same value: 0.72 ± 0.02 eV.*

of the spectra was actually in this transmission range, only much higher and lower. Again the reverse BEEM was very stable and 20 times lower than the direct BEEM.

4.2.3 15 min Ni deposition

The 15 min Ni deposition will result in a 11.3 nm thick $NiSi_2$ layer. Although there is one high BEEM transmission spectra ($\sim$ 30 pA/nA at -1.8 V), most spectra's are lower, around 20 pA/nA, see fig. 4.9. The reverse BEEM is ten times smaller than the forward BEEM, although there is a large spread in the spectra. At higher applied tip bias the spectra are not smooth. This reverse BEEM was not very stable and the values were fluctuating during the sweep, which resulted in a bad average. The SBH average of this sample is 0.71 ± 0.01 eV.

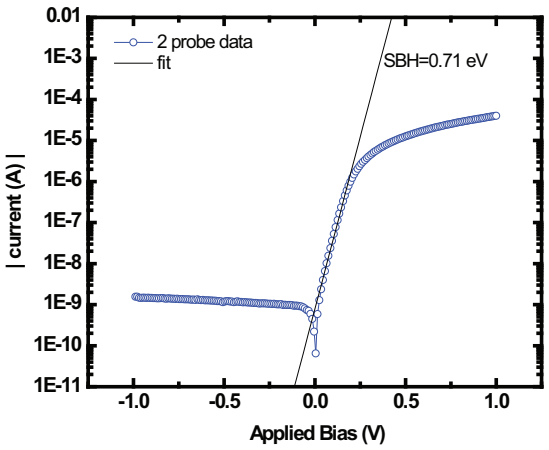

Figure 4.8: *The 2-probe measurement of the 10 min Ni deposition sample. The SBH is in this case 0.71 ± 0.01 and the ideality factor n=1.0.*

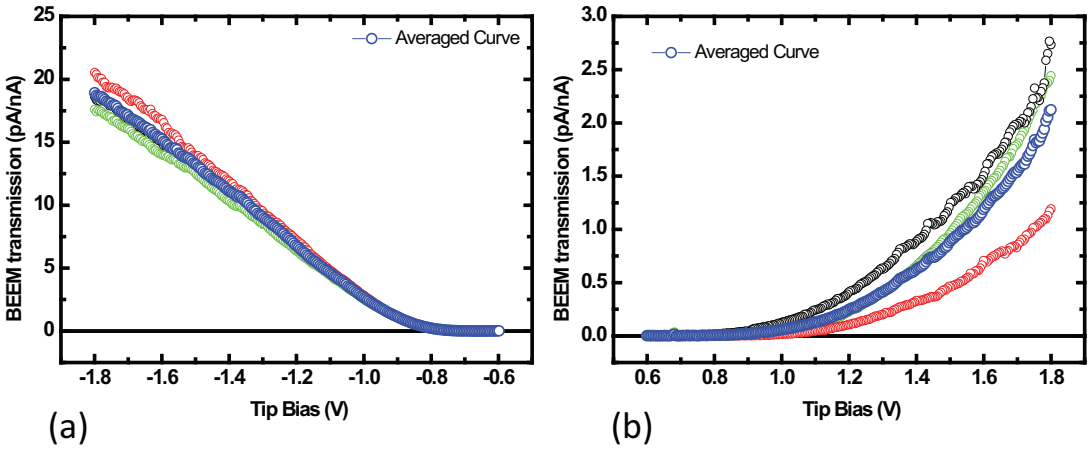

Figure 4.9: (***a***) *All Direct BEEM spectra for 15 min Ni deposition in one plot. The pink line is the average.* (***b***) *All Reverse BEEM spectra for 15 min Ni deposition in one plot. Again, the blue line is the average of all spectra.*

4.2.4 20 min Ni deposition

20 min of Ni deposition will result in a 15 nm $NiSi_2$ layer. The SBH is 0.69 ± 0.01 eV, which is slightly lower than the previous samples. The BEEM spectra can be seen in fig. 4.10. This sample shows in the spectra a large range of BEEM transmission in both the forward and reverse direction. The average is taken, the forward BEEM is again times larger than the reverse BEEM and the value at tip bias -1.8 eV is 17 pA/nA.

4.2.5 30 min Ni deposition

Because the SBH of the previous samples showed no change, it was decided to do a 30 min Ni deposition to create a 22.5 nm thick layer $NiSi_2$. If the SBH in this case would change, than the type of $NiSi_2$ would change. The SBH is in this case 0.67 ±

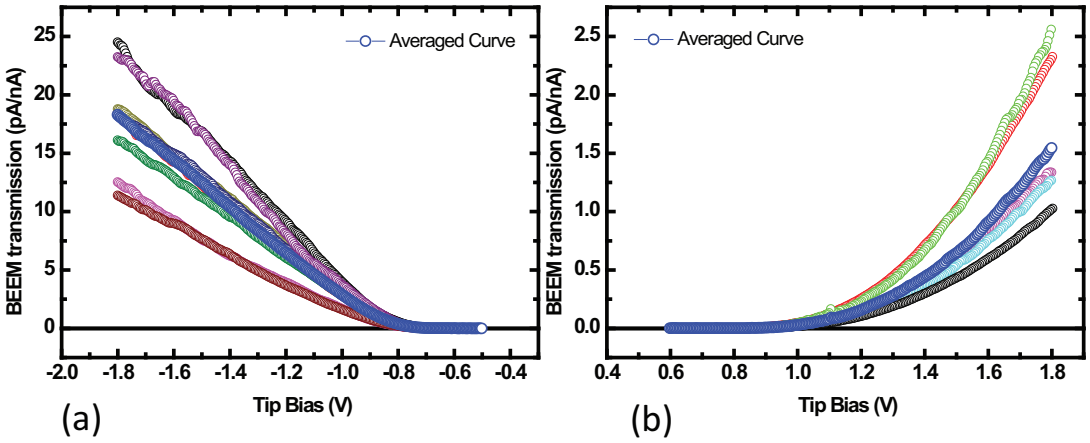

Figure 4.10: *The transmissions for the 20 min Ni deposition for* (***a***) *the direct BEEM and* (***b***) *the reverse BEEM. The average is the blue curve.*

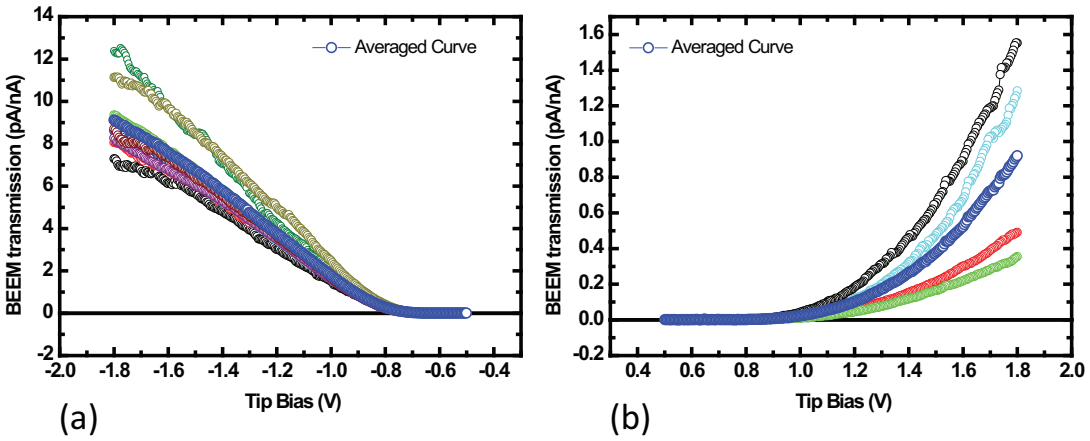

Figure 4.11: (***a***) *All Direct BEEM spectra for 30 min Ni deposition in one plot. The blue line is the average.* (***b***) *The average of the Reverse BEEM, blue, and all other spectra for 30 min Ni deposition.*

0.02 eV, which shows that it moves towards type-A SBH value of 0.65.

This 30 min Ni deposition sample shows a consistent direct BEEM transmission compared with the other samples. The value at -1.8 V is around 10 pA/nA and it is ten times higher than the reverse BEEM. The results can be seen in fig. 4.11. The reverse BEEM shows a large variation in spectra, but the average is consistent with the expectation from the previous results.

4.2.6 Schottky Barrier Height of $NiSi_2$ samples

The SBH's are also measured making use of plotting the square root of the transmission following eq. 2.7, these values of all sample can be found in the histogram in fig. 4.8a. The reverse BEEM SBH's were also measured, these values were only used to check whether the values are consistent, but are not presented here. Sometimes the reverse

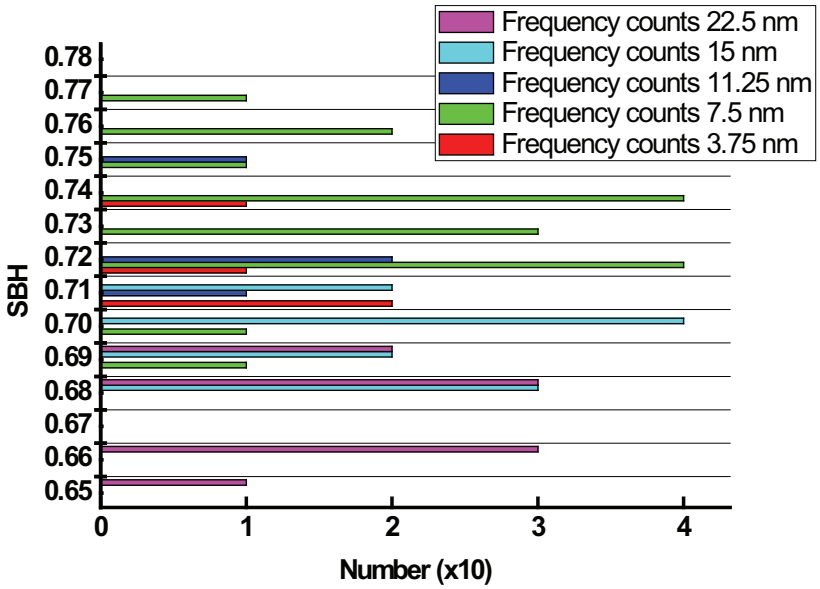

Figure 4.12: *Histogram of the SBH of all samples. The thicknesses are those of the $NiSi_2$ layer. Only the SBH of the direct BEEM are considered. The 22.5 nm thickness sample shows a lower SBH. Because the spectra shown in the figures below are averages of approximately 10 single spectra, the SBH is also an average of these spectra, so the total number is ten times larger*

BEEM SBH values showed a large deviation from the expected SBH, but that can be explained by the low BEEM transmission, where the power 1/4 had to be taken. This gave a certain freedom to draw the linear fit and derive the SBH. Also the SBH as an function of the deposited Ni thickness is given in figure 4.13. It can be seen that with increasing the Ni thickness the SBH decreased to the SBH value of Type-A $NiSi_2$ (0.65 eV). Since we have not performed the experiments at lower Ni thickness, we do not the phase of the $NiSi_2$ at those thicknesses. If our growth mode of $NiSi_2$ is the same as that described by Tung [19] *et al.* then for all the Ni thickness used in this work, we should end up with first a Type-A and at higher Ni thickness a mixed phase i.e in between that of Type-A and Type-B phase. However the growth protocol of Tung is strictly not identical to that of ours and thus a one to one correlation of the results cannot be done. It would be interesting to see if creating samples with thicker layers $NiSi_2$ (>22.5 nm) would change the type of $NiSi_2$.

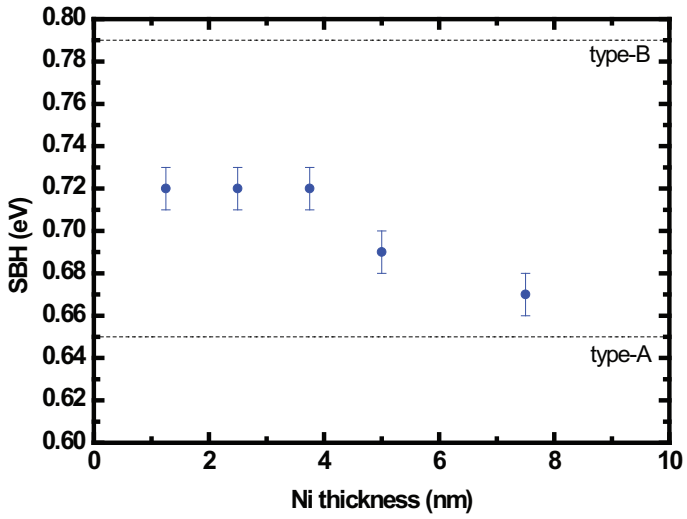

Figure 4.13: *The SBH as a function of the deposited Ni layer. The SBH of type-A and type-B are the dashed lines as reported. With an increasing thickness the SBH of our samples tend to go to type-A SBH.*

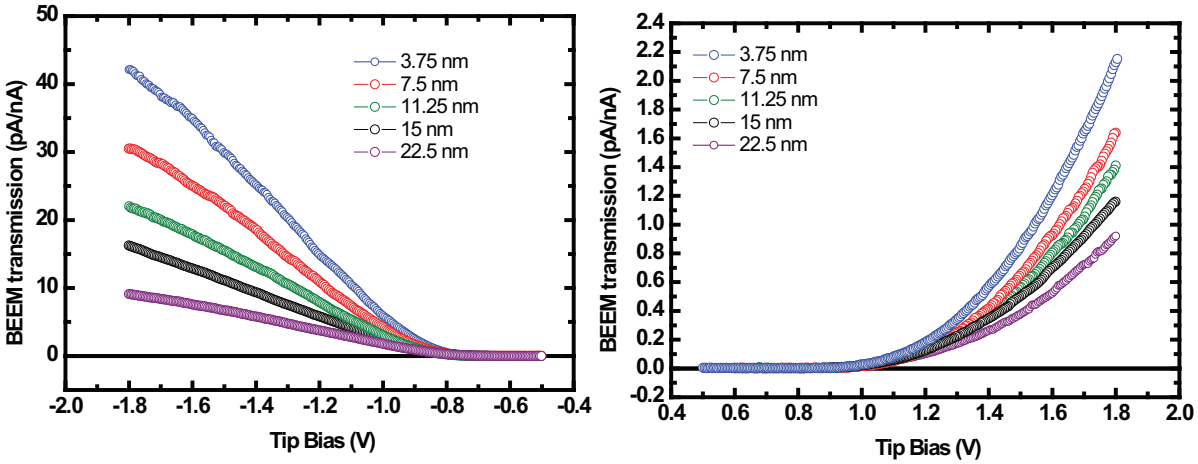

Figure 4.14: *The BEEM spectra of all the samples in one plot.* (***a***) *the direct BEEM.* (***b***) *the reverse BEEM.*

4.2.7 Attenuation length

By plotting the BEEM transmission versus the $NiSi_2$ thickness, the attenuation length can be extracted using eq. 2.4. For each applied tip bias between -1.8 V and -1.1 V the BEEM transmission was taken from fig. 4.14. This was done for each sample. The results are shown in fig. 4.15a. The BEEM transmissions at lower bias are not taken into account for deriving the attenuation length, because the signal to noise ratio is not adequate. Also the reverse BEEM attenuation length is done in the same manner, but now the values are from 1.2 V to 1.8 V. The reverse BEEM can be seen in 4.15b. The lines are fits following eq. 2.4. The data for higher energies could be fitted with

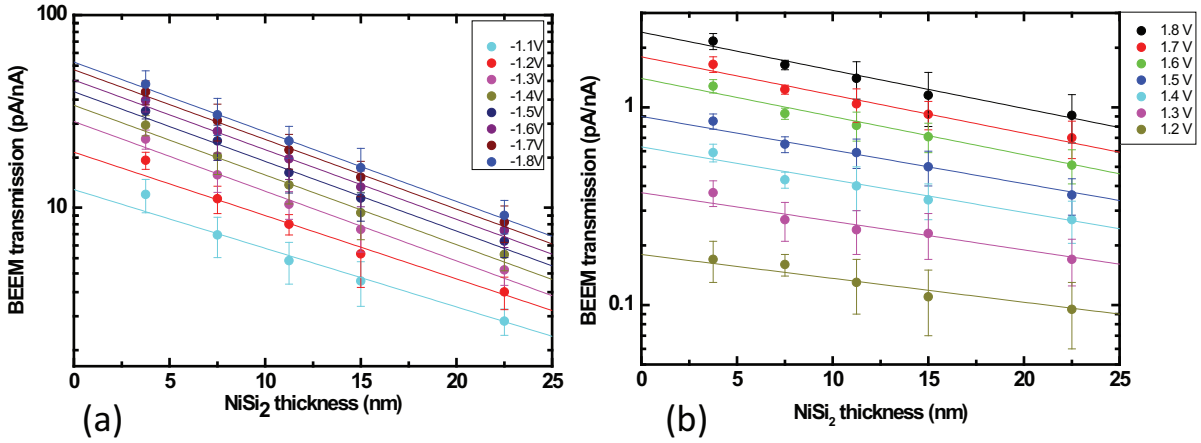

Figure 4.15: *BEEM transmissions as function of the thickness of the $NiSi_2$ layers in (**a**) the direct BEEM and (**b**) the reverse BEEM. The data points were taken for the same voltage. The fittings showed are eq. 2.4.*

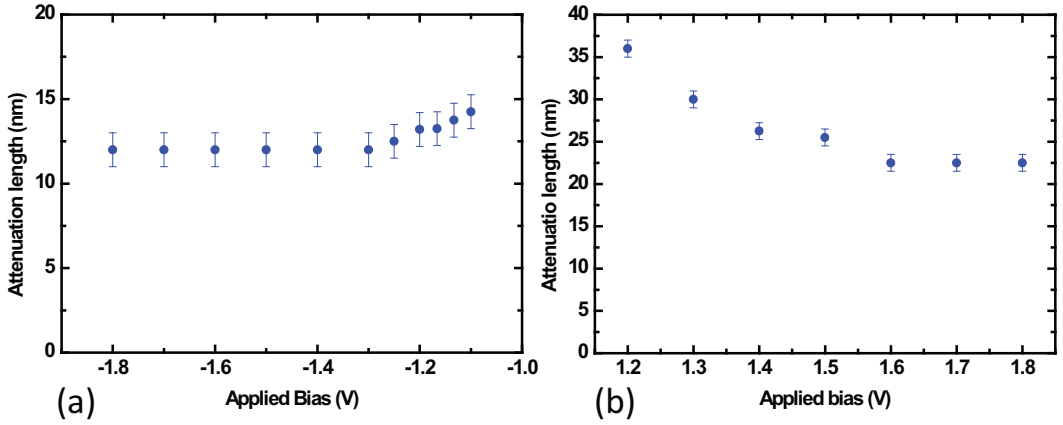

Figure 4.16: *The attenuation lengths as function of the applied tip bias for (**a**) the direct BEEM and (**b**) the reverse BEEM.*

the same λ, at lower energies this started to increase. The energy dependence of the attenuation lengths are given in fig. 4.16. Because there were only 5 data points, there was some freedom in the fitting parameters. That is why there is an error of 1 nm. From the BEEM measurements one can extract the value for λ. $\lambda = V_g\tau$, where V_g is the group velocity and τ is the inelastic lifetime. The density of electron states at higher energies can give an idea of the energy dependence of τ. An understanding of τ can be useful to understand the energy dependence of λ_i. The constant electron attenuation length between -1.8 V and -1.3 V is thought to arise due to a constant density of states at those energies. Fitting, as can be seen in fig. 4.17, was done using eq. 4.1 and with $E_F = 3.21$ eV, $\xi = 17$ and $\lambda_{fit} = 28$. The fit matches well at low energies but not at higher energies where strong electron-electron scattering influence the transport.

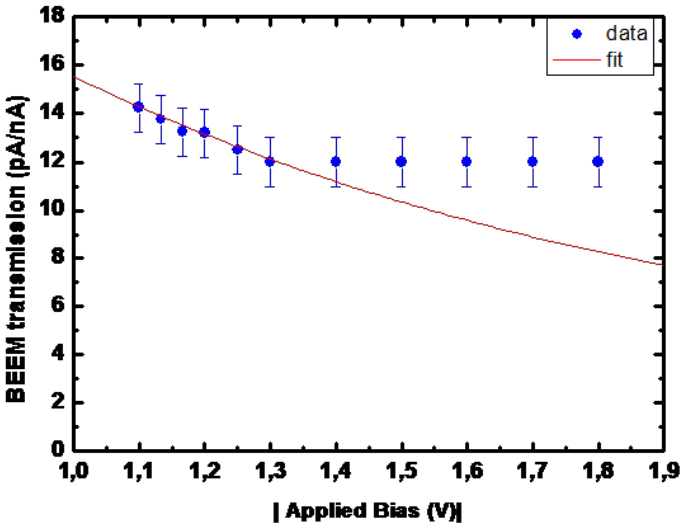

Figure 4.17: *Fitting of the data points, using the free electron model.*

$$\frac{1}{\lambda_a(E)} = \frac{1}{\lambda_i} + \frac{1}{\lambda_{fit}} = \frac{E^2}{\xi\sqrt{E+E_F}} + \frac{1}{\lambda_{fit}} \tag{4.1}$$

Comparing the attenuation length in the forward BEEM with the results of Lee [6] on $CoSi_2$, his results are almost 3× lower than our results for $NiSi_2$ (12 and 4 nm resp. at -1.8 V). This lower attenuation length means that the hot electrons in $CoSi_2$ scatter more than in $NiSi_2$. Another thing to remember is that the $NiSi_2$ is capped with gold. Between -1.2 and -0.9 V at 77 K the attenuation length of Au is 147 ± 6 Å[8], which is larger than the derived value for $NiSi_2$ so it will not have a big influence on the measurements.

Chapter 5

Conclusions

In this Bachelor thesis the hot electron attenuation length λ_a for $NiSi_2$ on top of n-Si(111) is reported for the first time. To achieve this two different things were done, first the preparation of flat passivated Si surfaces was investigated, thereafter the BEEM spectra of different samples with varying thicknesses $NiSi_2$ were collected and the attenuation length could be extracted from this.

The preparation of flat Si surfaces were needed to grow $NiSi_2$/Si interfaces with a low lattice mismatch. The roughness of the surfaces were examined with the AFM. The parameters that were researched and that needed to be optimized were the time for removing dissolved oxygen from the 40%NH_4F solution (bubbling) and the etching in this 40%NH_4F solution. The parameters could not be optimized for a 'new' substrate, because not enough data was collected to do reasonable statistics. It was shown that in some occasions, mostly with short bubbling times, etch pits were formed due to dissolved oxygen. This work for optimizing the parameters for the new Si substrate is still under construction. An old substrate, already used in previous experiments, was then examined. The wet chemical etch was done step by step and the surfaces roughness was checked again with the AFM. After the last step, etching in NH_4F, the RMS roughness of the surface of (1×1) μm is 4 Å, but on smaller scale the RMS roughess was around 2 Å. This result was good enough to grow epitaxially the $NiSi_2$. A drawback is that the reproducibility of this surface preparation is gone. Also the surface morphology after the chemical treatment is substrate dependent.

To calculate the hot electron attenuation length λ_a, samples of $NiSi_2$/n-Si(111) were prepared using MBE with different thicknesses $NiSi_2$. The thickness of $NiSi_2$ could be controlled with the initial layer thickness of Ni. Both direct and reverse BEEM spectra were taken. It is shown that the transmission decreased with increasing the layer thickness. From the BEEM transmissions of different samples at different applied biases the attenuation length was extracted. A plot of the transmission versus the $NiSi_2$ thickness showed that the transmission was $\propto \exp(-d/\lambda_a(E))$. Also the energy dependence of the attenuation length was derived. This data was fitted with the free electron theory and was seen to match well with a E_F of 3 eV for lower energies but not at higher energies. A difference in the increase of the λ_a at a different bias could be explained with the DOS at higher energies. To check whether the same type of $NiSi_2$

was grown, the SBH of the samples was measured with a fit of the square root of the transmission versus the thickness. The values for the SBH showed a constant value for the SBH of 0.73 ± 0.01 eV up to a layer thickness of 5 nm Ni thickness. Thereafter a slight decrease in the SBH is seen, but at a higher thickness than reported by Tung [19]. The SBH seems to tend to type-A.

Acknowledgments

This Bachelor project is not only 'my' project. In fact, I could not have done anything without the help of many people, and I should thank them here.

The first person I would like to thank is my direct supervisor Subir Parui for letting me participate in his PhD research. He did the sample preparation, I was observing him during the chemical treatment in the NanoLab and the MBE deposition.

The next person to acknowledge is dr. Tamalika Banerjee for accepting me in her group and for being my supervisor. Also the discussions with her contributed a lot this work.

I should thank Petra Rudolf for the usage of the MBE system.

Thanks to the technicians Martijn de Roosz, Bernard Wolfs and especially Johan Holstein for letting me use the NanoLab.

Also thanks to K. Gaurav Rana, Jan van der Ploeg and Seva Khikhlovskyi for their contributions in the weekly group discussions.

I would like to express my gratitude to Bart van Wees for being the referent of this Bachelor Thesis.
Thanks to all members of the FND and to the students in the 'studentenkamer'.

Bibliography

[1] S. Parui, B. Wit, L. Bignardi, P. Rudolf, B. Kooi, B. J. van Wees, and T. Banerjee. Hot electron transmission in metals using epitaxial $NiSi_2$/n-Si(111) interfaces. *Appl. Phys. Lett.*, **99**(3):032104, 2011.

[2] W. J. Kaiser and L. D. Bell. Direct investigation of subsurface interface electronic structure by ballistic-electron-emission microscopy. *Phys. Rev. Lett.*, **60**(14):1406–1409, April 1988.

[3] L. D. Bell and W. J. Kaiser. Ballistic-electron-emission microscopy: A nanometer-scale probe of interfaces and carrier transport. *Annu. Rev. of Mater. Sci.*, **26**:189–222, 1996.

[4] M.D. Stiles and D.R. Hamann. Theory of ballistic electron emission spectroscopy of $NiSi_2$–Si(111) interfaces. *Materials Science and Engineering: B*, **14**(3):291–296, August 1992.

[5] M. D. Stiles and D. R. Hamann. Theory of ballistic-electron-emission spectroscopy of $NiSi_2$/Si(111) interfaces. *Phys. Rev. Lett.*, **66**(24):3179–3182, June 1991.

[6] E. Y. Lee, H. Sirringhaus, U. Kafader, and H. von Känel. Ballistic-electron-emission-microscopy investigation of hot-carrier transport in epitaxial $CoSi_2$ films on Si(100) and Si(111). *Phys. Rev. B*, **52**(3):1816–1829, July 1995.

[7] J. J. Garramone, J. R. Abel, I. L. Sitnitsky, L. Zhao, I. Appelbaum, and V. P. LaBella. Measurement of the hot electron attenuation length of copper. *Appl. Phys. Lett.*, **96**(6):062105, 2010.

[8] C. A. Ventrice, V. P. LaBella, G. Ramaswamy, H. P. Yu, and L. J. Schowalter. Measurement of hot-electron scattering processes at Au/Si(100) schottky interfaces by temperature-dependent ballistic-electron-emission microscopy. *Phys. Rev. B*, **53**(7):3952–3959, February 1996.

[9] L. D. Bell, M. H. Hecht, W. J. Kaiser, and L. C. Davis. Direct spectroscopy of electron and hole scattering. *Phys. Rev. Lett.*, **64**(22):2679–2682, May 1990.

[10] S. M. Sze. *Physics of Semiconductor Devices.* Wiley, New York, 1981.

[11] Ehtsham-Ul-Haq. *Nanoscale spin-dependent transport of electrons and holes in Si-ferromagnet structures.* PhD thesis, Univ. Twente, 2005.

[12] G. S. Higashi, R. S. Becker, Y. J. Chabal, and A. J. Becker. Comparison of si(111) surfaces prepared using aqueous solutions of nh$_4$f versus hf. *Appl. Phys. Lett.*, **58**(15):1656–1658, April 1991.

[13] Hiroki Kato, Takumi Taoka, Shozo Suto, Susumu Nishikata, Gen Sazaki, Kazuo Nakajima, Taro Yamada, Ryszard Czajka, Andrzej Wawro, and Atsuo Kasuya. Preparation and characterization of ultraclean H:Si(111)-(1x1) surfaces studied by HREELS, AFM and STM-STS. *e-Journal of Surface Science and Nanotechnology*, **7**:557–562, 2009.

[14] G. J. Pietsch, U. Kohler, and M. Henzler. Anisotropic etching versus interaction of atomic steps: Scanning tunneling microscopy observations on HF/NH_4F-treated Si(111). *J. Appl. Phys.*, **73**(10):4797–4807, May 1993.

[15] Gregor S. Hsiao, Jorma A. Virtanen, and Reginald M. Penner. Scanning tunneling microscopy investigations of the Si(111) topography produced by etching in 40% NH_4F: Observation of an optimum etch duration. *Appl. Phys. Lett.*, **63**(8):1119–1121, August 1993.

[16] Philippe Allongue, Catherine Henry de Villeneuve, Sylvie Morin, Rabah Boukherroub, and Danial D. M. Wayner. The preparation of flat H-Si(111) surfaces in 40% NH_4F revisited. *Electrochimica Acta*, **45**(28):4591–4598, October 2000.

[17] Hirokazu Fukidome and Michio Matsumura. Electrochemical study of atomically flattening process of silicon surface in 40% NH_4F solution. *Applied Surface Science*, **130**:146–150, June 1998.

[18] R. T. Tung. Schottky-barrier formation at single-crystal metal-semiconductor interfaces. *Phys. Rev. Lett.*, **52**(6):461–464, February 1984.

[19] R. T. Tung, J. M. Gibson, and J. M. Poate. Formation of ultrathin single-crystal silicide films on Si: Surface and interfacial stabilization of Si-$NiSi_2$ epitaxial structures. *Phys. Rev. Lett.*, **50**(6):429–431, February 1983.

[20] K.Y. Gao and B.X. Liu. Formation of high-conductivity $NiSi_2$ layers on Si at zero-mismatch temperature by high-current Ni-ion implantation. *Applied Physics A: Materials Science & Processing*, **68**(3):333–337, 1999.

[21] R.T. Tung, J.M. Poate, J.C. Bean, J.M. Gibson, and D.C. Jacobson. Epitaxial silicides. *Thin Solid Films*, **93**(1-2):77–90, July 1982.

[22] R. T. Tung, J. M. Gibson, and J. M. Poate. Growth of single crystal epitaxial silicides on silicon by the use of template layers. *Appl. Phys. Lett.*, **42**(10):888–890, May 1983.

[23] R. T. Tung, K. K. Ng, J. M. Gibson, and A. F. J. Levi. Schottky-barrier heights of single-crystal nisi2 on si(111): The effect of a surface p-n junction. *Phys. Rev. B*, **33**(10):7077–7089, May 1986.

[24] Takahiro Suzuki and Sadao Adachi. Chemical treatment effect of Si(111) surfaces in NH_4F solution studied by spectroscopic ellipsometry. *Japanese Journal of Applied Physics*, **33**(Part 1, No. 10):5599–5602, 1994.

[25] Jian Hua Ouyang, Xin Sheng Zhao, Ting Li, and Da Cheng Zhang. Direct measurement of the etching rates on Si (111) and silicon dioxide surfaces in 40% ammonium fluoride aqueous solution via atomic force microscopy. *J. Appl. Phys.*, **93**(7):4315–4320, April 2003.

[26] C. R. Crowell, W. G. Spitzer, L. E. Howarth, and E. E. LaBate. Attenuation length measurements of hot electrons in metal films. *Phys. Rev. Lett.*, **127**(6):2006–2015, September 1962.